Three-Dimensional Numerical Analysis and Optimization of Electromagnetic Suspension System for 200 km/h Maglev Train Considering Eddy Current Effect

JINGFANG DING[1], XIN YANG[1], ZHIQIANG LONG[1], AND NING DANG[2]
[1]Maglev Research Centre, National University of Defense Technology, Changsha 410000, China
[2]Hunan Maglev Technology Research Center, Changsha 410000, China

Corresponding author: Xin Yang (yangxin.cambridge@foxmail.com)

ABSTRACT Electromagnetic suspension (EMS) is an important type of maglev train systems. With commercial success in the low-speed maglev train, developing a medium-speed maglev type with a top speed of 200 km/h based on the current low-speed maglev technology has been attracting great research interest and engineering effort. This new maglev system will nicely meet the requirement of inter-city transportation. However, at a higher speed, the eddy current effect in the EMS system of the leading end of a maglev train becomes an unnegligible factor, as the induced eddy current in the non-laminated steel rails will tremendously reduce the levitation force. This paper comprehensively investigates the mechanism of eddy current effect in the EMS system and uses a 3-D finite-element method to fully analyze the impacts of eddy current on levitation force adopting an accurate simulation model. Compared with the experimental data, the simulation results show good agreement. With this accurate simulation model, an optimized design of an electromagnetic levitation system is proposed as well as its corresponding control scheme. The proposed design at 200 km/h effectively mitigates the eddy current effect while still maintaining the required levitation force at the leading end of maglev train.

INDEX TERMS Eddy current effect, finite element method, EMS, electromagnet module, medium-speed maglev train.

I. INTRODUCTION

Maglev technology is widely used in maglev train [1] and magnetic bearing [2]–[5] due to its special advantages of using levitation force to overcome gravity. In recent years, maglev trains have made considerable breakthroughs in the world. EMS maglev train is such a kind of modern transportation that has great advantages of low noise, high efficiency and ride comfort. This type has achieved great success in low-speed (100 km/h) and high-speed (450 km/h) maglev trains. The main state-of-the-art maglev train technologies include Korean UTM, Japanese HSST and German Transrapid [1], [6], [7]. In China, Changsha Maglev Express (CME), as the longest low-speed maglev commercial demonstration line of the world, was officially put into operation

in 2016. It adopts a similar approach as the HSST and UTM by using EMS for levitation and SLIM (Short-primary Linear Induction Motor) for propulsion. The levitation and propulsion systems are separated to reducing the number of electromagnets and controllers while the guiding force is automatically generated from the EMS system. This low-speed maglev train has extra merits of nice climbing ability, small turning radius and low construction cost. Its maximum design speed is 100 km/h.

In spite of heated research effort in high-speed maglev trains [7]–[10], there is also ongoing research on a 200 km/h medium-speed maglev train for inter-city travel in the world [11]–[13]. The earliest low-speed maglev train (Japanese HSST) is believed to be capable to run up to

200 km/h. However, it needs to consider the guidance capability as it is now being developed in [11] and [12]. There is still no experimental test or thorough simulation analysis to prove that this maglev train of 200 km/h can be operated normally.

Furthermore, the eddy current effect, which is comprehensively investigated in [14] to build a new nonlinear lumped parameter equivalent circuit model, in the EMS system of the leading end of a maglev train becomes an unnegligible factor in case of higher velocities as it would not only reduce the levitation force but also produce a drag to the propulsion system [15]. For widely-used non-laminated steel rails in all the low-speed maglev systems, moving levitation electromagnet easily induces eddy current in the rails. A theoretical analysis was carried out in [16] which equates the three-dimensional Maxwell's equations with the two-dimensional Laplace's equation in order to evaluate the weakened magnetic field of the air gap, and utilizes the Maxwell stress tensor method to calculate the reduced levitation force. In [15], FEM was made to further calculate the weakened levitation force. Both studies concluded that with the increase of operation speed the levitation force would be considerably reduced. However, both studies simplified the analysis or decrease the computation costs by utilizing simplified models that treat both electromagnet and rail as a simple U shape, without taking into account the actual shape of plates, cores and rail, as well as the grooves for mounting, cooling and weight reduction. This considerably undermines the accuracy of calculation. To achieve a reasonable maglev train design of 200 km/h developed from the low-speed maglev technology available, more accurate analysis and more effective solutions for eddy current effect in EMS is of great necessity.

II. EDDY CURRENT EFFECT IN EMS MAGLEV SYSTEM

1) EMS MAGLEV SYSTEM

Fig.1(a) demonstrates the cross-sectional schematic of the EMS-SLIM maglev system developed in CME, which is very similar to the structure of low-speed maglev trains shown in [11]–[13] and [16]. The EMS maglev system consists of electromagnet modules mounted on bogies and F-rails. The SLIM could be seen as its primary side installed on the bogie and its secondary side, the reaction plate, is put on the top of the F-rail. The actual side view of a bogie is also shown in the left of Fig.1(a). In this paper, we will use this maglev type as the medium-speed maglev type for the rest discussion.

The maglev train of CME has three carriages, including one middle carriage (M car) and two head carriages (MC1 and MC2 carriages), which can run in both directions. As illustrated in Fig.1(b), each carriage contains ten electromagnet modules, five on each side. One pair of two electromagnet modules paralleled on both sides of the carriage is installed on a mechanical bogie which is used to decouple the mutual mechanical coupling between the paired electromagnet modules. In this way, the suspension control of each electromagnet module will become independent to each other [13].
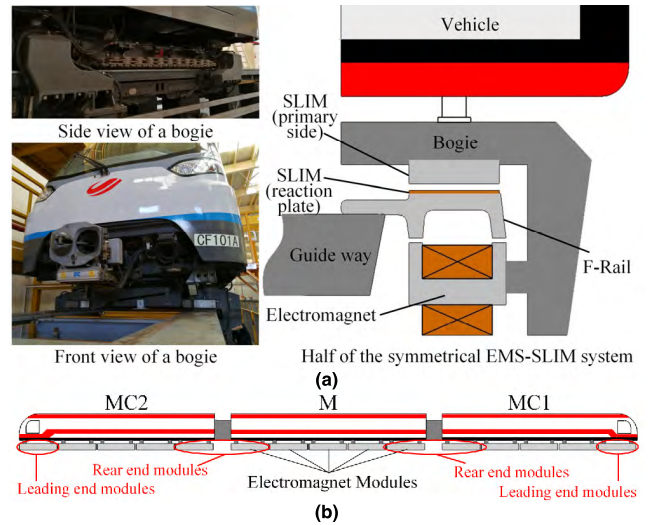

FIGURE 1. (a) Cross-sectional view of CME maglev train, (b) Simplified model of CME maglev train.

There are four coils in every electromagnet module of the low-speed CME maglev train, two of which form a levitation control point controlled by the same levitation current as illustrated in Fig.2(a). It is named two-controller system. The two-controller system can be simplified into two independent single-levitation-point models for analysis and controller design [17], [18]. Each single levitation point model can be described as Fig.2(b). The system equations of the levitation system are shown in formula (1). It contains dynamic equation, electrical equation, electromagnetic equation and boundary condition, which is similar to the levitation principle of magnetic bearing [19].

$$\begin{cases} m\ddot{z} = (M + m)\, g - F\,(i, z) + f_{\mathrm{d}} \\ u \approx Ri + \dfrac{\mu_0 N^2 A}{2} \cdot \dfrac{\dot{i}}{z} - \dfrac{\mu_0 N^2 A i}{2} \dfrac{\dot{z}}{(z)^2} \\ F\,(i, z) = \dfrac{\mu_0 N^2 A}{4} \left(\dfrac{i}{z}\right)^2 \\ mg = F\,(i_0, z_0) = \dfrac{\mu_0 N^2 A}{4} \left(\dfrac{i_0}{z_0}\right)^2 \end{cases} \quad (1)$$

Where, z is the height of air gap between electromagnet and track, m and M are the equivalent mass of electromagnet and vehicle respectively, $F\,(i, z)$ is the electromagnetic force, i is the levitation current in coil, f_{d} is the interference force, u is the control voltage, R is the impedance, N is the number of turns, A is the area of electromagnet pole, μ_0 is the vacuum magnetic conductivity, i_0 and z_0 are respectively the current of the coil and the height of the air gap at static state. In addition, some assumptions were made, including the average magnetic potential over the air gap, zero magnetic reluctance on the iron core and rail, zero magnetic leakage, endless end effect, and force centers coincided with geometric centers.

By linearizing the dynamic equations at the equilibrium point, the system can be easily analyzed and the controller can be designed. The state feedback controller is often used
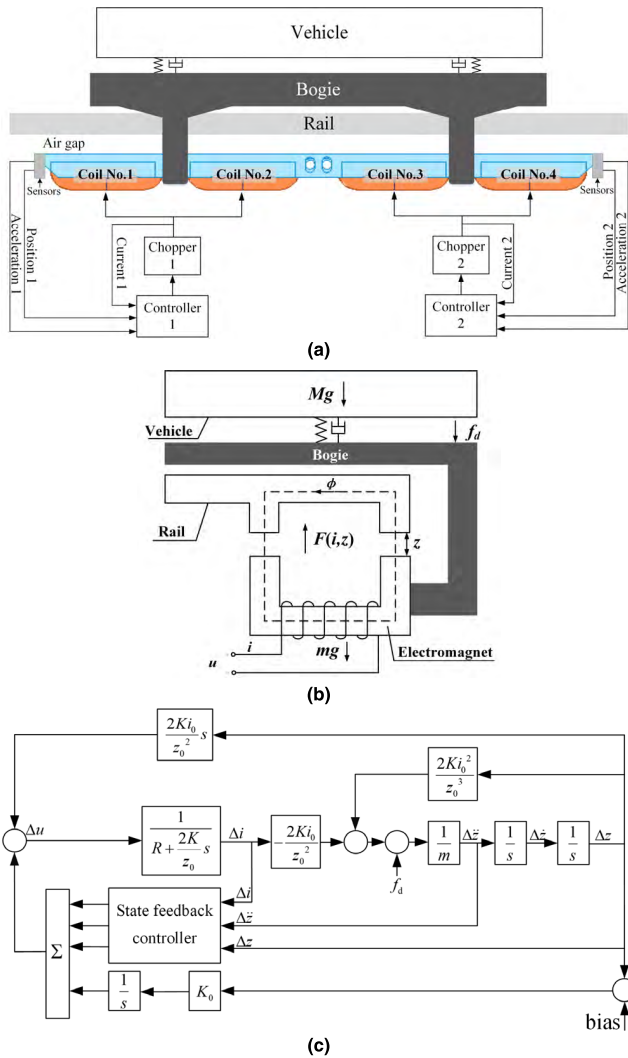
(a)

(b)

(c)

FIGURE 2. (a) Two-controller levitation system, (b) Single levitation point model, (c) Control block diagram of levitation system.

(a)

(b)

FIGURE 3. (a) Exploded view of magnetic flux in rail, (b) Magnetic equivalent circuit of EMS.

in the research of levitation control [20], [21]. Fig.2(c) is a control block diagram of levitation system, which applies state feedback controller to gap feedback, current feedback and acceleration feedback. Besides, the integral feedback of gap deviation is also taken into account to eliminate the steady-state error.

The eddy current effect as reported in [15] and [16] mainly appears at the leading end of the electromagnet module in MC1 or MC2 carriage dependent on the operation direction which is proved later.

2) THE MECHANISM OF EDDY CURRENT EFFECT

When maglev train moves, the magnetic field of air gap established between electromagnet modules and rail moves along the rail, and a new magnetic field will be formed in the rail and air gap ahead of the train. According to the Faraday law of electromagnetic induction, such an emerged magnetic field from the head electromagnet modules will
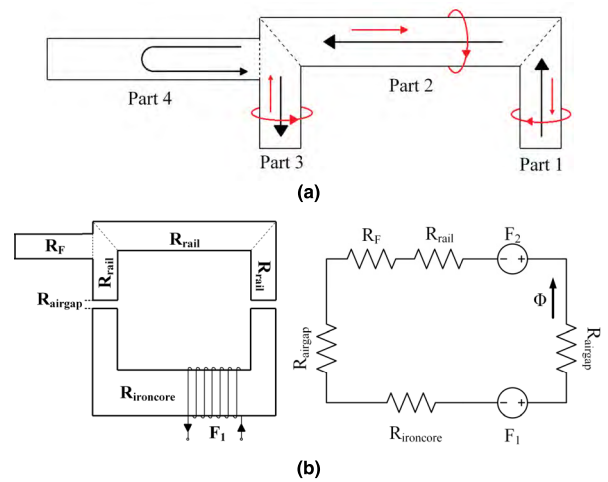
produce an eddy current in the non-laminated steel rail due to the enhanced magnetic field. This eddy current generates a magnetic field in the opposite direction, preventing the magnetic field in the rail from increasing. Therefore, the air gap magnetic flux is weakened and the levitation force is reduced. At the end of the electromagnet modules the train moves away from the previous magnetic field, the eddy current prevents the magnetic field in the rail from decreasing. As only the eddy current at the front has serious influence on the levitation force, the overall levitation force decreases. This paper mainly analyses the eddy current effect at the front end.

The magnetic flux density's direction can be simply illustrated in Fig.3(a). The F-rail is divided into four parts. The black arrows indicate the directions of magnetic flux density generated by the electromagnet module. The red straight arrows explain the directions of magnetic flux density generated by the eddy current. According to the Ampere's right-hand rule, the direction of eddy current can be judged as red circular arrows show. This is a simplified graph to demonstrate what the expected eddy current would look like.

The magnetic circuit method can also be used to prove the reduction of air gap magnetic flux, as shown in Fig.3(b). The magnetic field is considered to be approximately stable when the train runs at a constant speed. F_1 and F_2 are the magnetomotive forces provided by the electromagnet and eddy current respectively. The magnetic reluctances are connected in series. R_{airgap} represents magnetic reluctance of the air gap. $R_{ironcore}$ represents magnetic reluctance of the iron core and plate. R_{rail} represents magnetic reluctance of the Part 1, 2 and 3 of the F-rail. R_F is the magnetic reluctance of the Part 4 of the F-rail. According to the magnetic circuit Ohm's law, the following equation can be obtained:

$$F_1 - F_2 = \left(R_{airgap} + R_{ironcore} + R_{rail} + R_F \right) \Phi \qquad (2)$$

where F_1 is the product of coil turns and current value

$$F_1 = Ni \quad (3)$$

The magnetic reluctance R_{airgap}, $R_{ironcore}$ and R_{rail} (All represented by R_m) depend on magnetic permeability μ, length l and cross-sectional area of magnetic path S:

$$R_m = l/\mu S \quad (4)$$

Φ is the magnetic flux, B is the magnetic flux density:

$$\Phi = BS \quad (5)$$

Since F_2 reduces F_1 when the train moves, the magnetic flux Φ and the magnetic flux density of air gap decreases. However, such a simplified equation cannot take the fringing effects of magnetic flux and 3-D structural of the rail into account [8]. In the following sections, 3-D numerical analysis method is further used to comprehensively analyze the eddy current effect.

III. 3-D NUMERICAL SIMULATION

A. 3-D FEM

According to the structure, size and parameters of CME, Maxwell software is used to implement the 3-D numerical analysis of EMS system, which is one type of electromagnetic simulations by using FEM based on Maxwell's differential equation. The principle is to transform electromagnetic calculation into a large matrix solution by discretizing the whole solution region. In order to calculate a more accurate model, a 64-core workstation with a RAM of 128 GB is used for simulation. The CPU is Intel(R)Xeon(R) CPUe5-2697v3@2.60GHz. The simulation method includes the following important processes:

1) Selecting solution type

The simulation type mentioned in this paper is transient analysis, since the transient simulation can solve the motion problem. The operation involved in medium-speed maglev train is mainly linear motion at a constant speed. The expected result is the segment where the simulation goes into the steady state so the transient analysis is selected.

2) Building the model

The 3-D model is established as shown in Fig.4. The structure and size are 1:1 in proportion to CME's electromagnet module. The single electromagnet module consists of an inner plate, an outer plate, four iron cores and four coils (each coil labeled in Fig.4(a)). The thickened portions of the plates used to mitigate magnetic saturation is considered. The ventilating slots for cooling, the slider notches, the chamfers for sensor installation, the mounting holes for brake clamps, and the slots for reducing weight are also involved. The rated air gap is 10 mm. The weight of the electromagnet module is 400 kg.

3) Choosing the Materials

The material of the guide rail, iron core and plate is non-laminated steel material, Q235B. The B-H curve of Q235B is shown in Fig.5(a). Its nonlinearity is considered, and the saturated magnetic flux density of Q235B is about 1.4 T. The coil
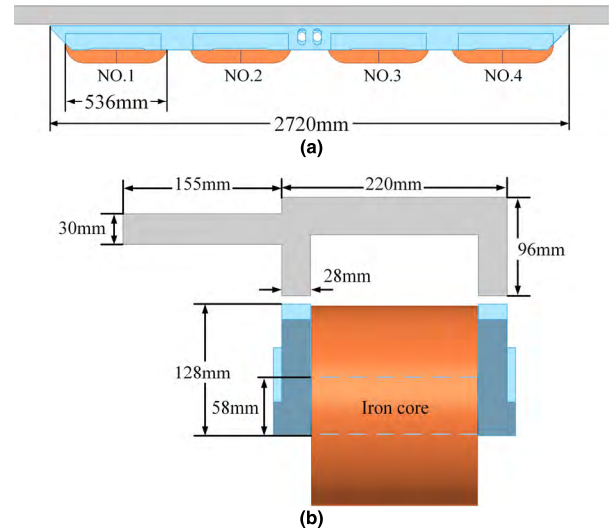

FIGURE 4. (a) The side view of a single 3-D electromagnet module, (b) The cross-section view of a single 3-D electromagnet module.
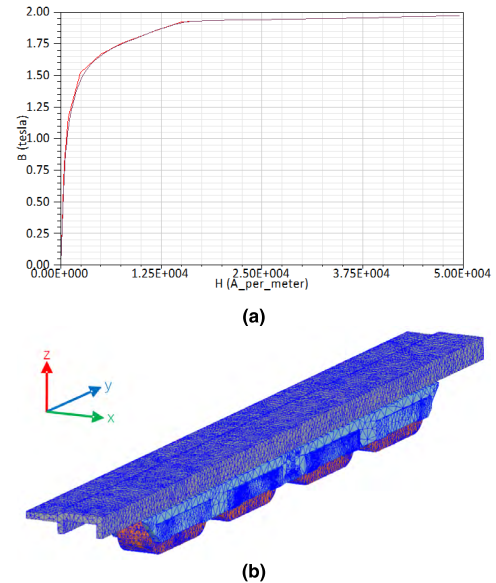

FIGURE 5. (a) B-H curve of Q235B, (b) Mesh view of model.

material is particularly chosen to be aluminum because of its light weight, low cost and good electrical conductivity.

4) Defining the Boundary

"Region" boundary, whose faces are zero field boundaries, is adopted. All the models and magnetic fields are included in the "Region".

5) Adding the Excitation

The excitation of 3-D simulation needs to be added on the coil terminals (the cross-section of the coil). A DC current excitation is used. The coil terminals are added to the windings. Turns and current values can be set on the windings where the number of turns is 360 and the rated current is 35 A. The rail as our analysis target needs to be selected to do eddy current calculation.

6) Setting the Motion

It should be noted that the object in the motion space must be an entity. Since the current cannot be added as an entity but a sheet, the electromagnet module is excluded in the motion space. Therefore, the rail is used as a moving object whose direction of motion is the y-axis positive direction. Firstly, the motion space is set outside the rail, which is a rectangle surrounding the F-rail and the movement track. Secondly, the motion mode is set to be linear while the motion direction, distance and speed are also set on the motion space.

7) Planning the Mesh

The more meshes the model is divided into, the more accurate the calculations will be. When the number of meshes is increased to a certain value, the calculated results will no longer be influenced. However, the number of meshes is limited by the capability of the computer. We use the combination of manual division method and automatic division method. Fig.5(b) is the mesh schematic of this simulation with a total number of about 250,000 meshes at 0 km/h, among which the coils take up about 35,000, the plates and iron cores take up about 25,000, the F-rail takes up about 50,000 and the rest is distributed to the motion space and ''Region''. When the train is moving, a longer rail model is required, in which case the number of meshes for the rail can be more than 100,000 and the total number of grids can be up to 400,000.

8) Setting up the solution

The time step and the stop time of each simulation need to be set. The motion space is defined previously. When the electromagnet module stops (no eddy current), it costs 5ms for the model to become steady. In this case, the selection of time step has little influence on the result. However, when the electromagnet module moves, the smaller the time step, the more accurate the calculation. Considering the calculation cost, the time step of this simulation is chosen to 1 ms. Under different running speeds different steady times for the model are required to reach stability. The faster the speed, the less steady time it takes. When the speed is 200 km/h, the steady time is 90 ms. When the speed is 60 km/h, the steady time is 300 ms. In order to obtain accurate results, the stop time needs to be greater than the steady time. For a single simulation (for example, 200 km/h case), it takes about 60 hours to complete each running of simulation.

B. 3-D NUMERICAL ANALYSIS SCHEME: U-RAIL v.s. F-RAIL

The actual rail of EMS maglev system is F-rail. Although many studies use U-rail as a simplified model to analyze the eddy effect saving great amount of computation costs, F-rail is more accurate. In this paper, we compared the simulation results of U-rail with those of F-rail. The model with U-rail uses the same design parameters except Part 4 as shown in Fig.3(a). Fig.6 indicates the FEM results. When the train is levitated without moving, it can be seen that in Part 4 there is little magnetic flux. However, if the train moves at 90 km/h, there will be plenty of magnetic flux induced in Part 4.
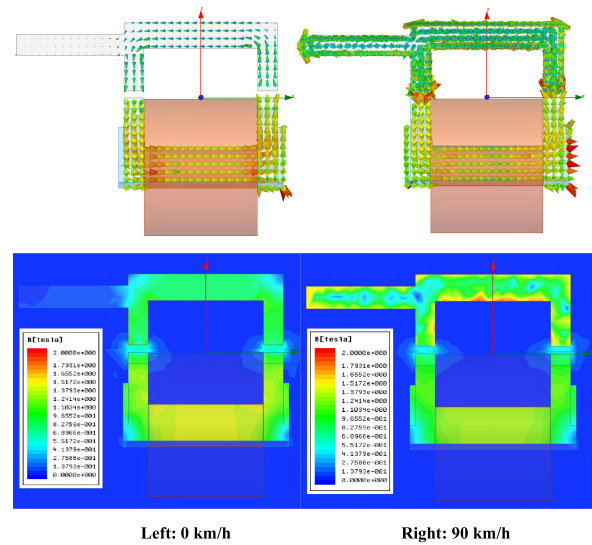

Left: 0 km/h   **Right: 90 km/h**

FIGURE 6. FEM results of magnetic flux vector (top) and magnetic flux density (bottom) in cross-section view.

Therefore, it is crucial to take the full F-rail into account when analyzing the eddy currents, which is performed in the following analysis. The comparison of forces between U-rail and F-rail at different speeds is given later.

IV. SIMULATION AND EXPERIMENTAL RESULTS
A. SINGLE-MODULE RESULTS

In this paper, we consider the AW0 load condition (empty train without any passenger). Each carriage of CME weighs 24 tons. Each section contains 10 elelctromagnetic modules, which requires on average a force output of around 24 kN per module. The static levitation current of AW0 is 28 A.

By utilizing the FEM, the simulation results of eddy current, magnetic field and force can be obtained. Fig.7(a) shows global and local view of the current density and direction at 90 km/h. It can be seen from the global view that the eddy current is mainly distributed in the position of the F-rail which corresponds to both ends of the electromagnet module. The directions of eddy currents at both ends are reverse. The side view is the y-z plane that viewed from the positive direction to the negative direction along the x-axis. The bottom view is the x-y plane that viewed from the negative direction to the positive direction along the z-axis. The eddy current directions of Part 1, Part 2 and Part 3 in this figure are the same as those in Fig.3(a), which verifies the mechanism of eddy current effect.

In order to analyze the eddy current effect at different speeds, five cases of speeds (0 km/h, 60 km/h, 90 km/h, 160 km/h and 200 km/h) are considered. Fig.7(b) illustrates the eddy current density J_x (in the x-axis) of a line along the y-axis in Part 1 of the rail. Its horizontal axis is the y-coordinate value of the line, where, y = 0 corresponds to the front of electromagnet module, y = 2720 corresponds to the end of electromagnet module. From Fig.7(b), the opposite
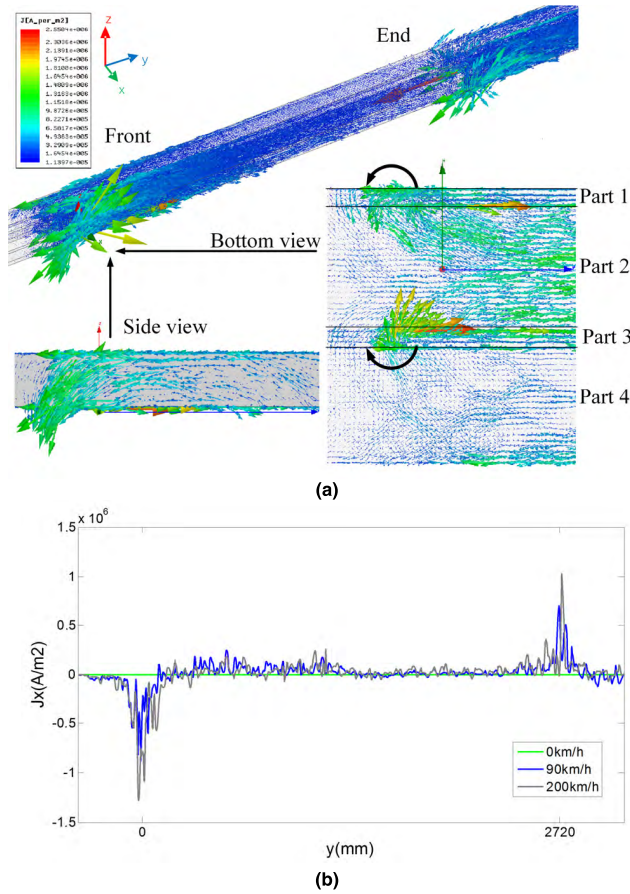
FIGURE 7. (a) Eddy current in the rail (b) Eddy current density of the rail in x-direction.

eddy current corresponding to the both ends of the electro-magnet module can be seen more clearly. With the increase of speed, the induced eddy current also increases greatly at both ends of the single electromagnet module.

The magnetic flux density B_z (in the z-axis) of a line along the y-axis in the air gap are shown in Fig.8(a). Due to the presence of eddy current, The magnetic flux density at the front decreases considerably with the increase of speed from 0 km/h to around 90 km/h. This reduction trend remains before the middle of the electromagnet module (around y = 1350 mm). Above 90 km/h, the magnetic flux density reduction becomes comparatively smaller as it can be seen from the curves from 90 km/h to 200 km/h. Comparing the curves of 160 km/h and 200 km/h, we can hardly observe significant reduction as observed previously.

Fig.8(b) shows the magnetic flux density inside iron cores of the four coils. Interestingly, the reduction is also significant, suggesting that the eddy current effect affects magnetic fields not only in air gap and rail, but also in iron cores. For the first two coils, the magnetic flux density drops from around 1.4 T to 1.2 T, from 0 km/h to 160 km/h. Similarly, the reduction from 160 km/h to 200 km/h is less significant. For the left two coils, the trend is similar, however, the reduced values become much smaller as it can be seen.
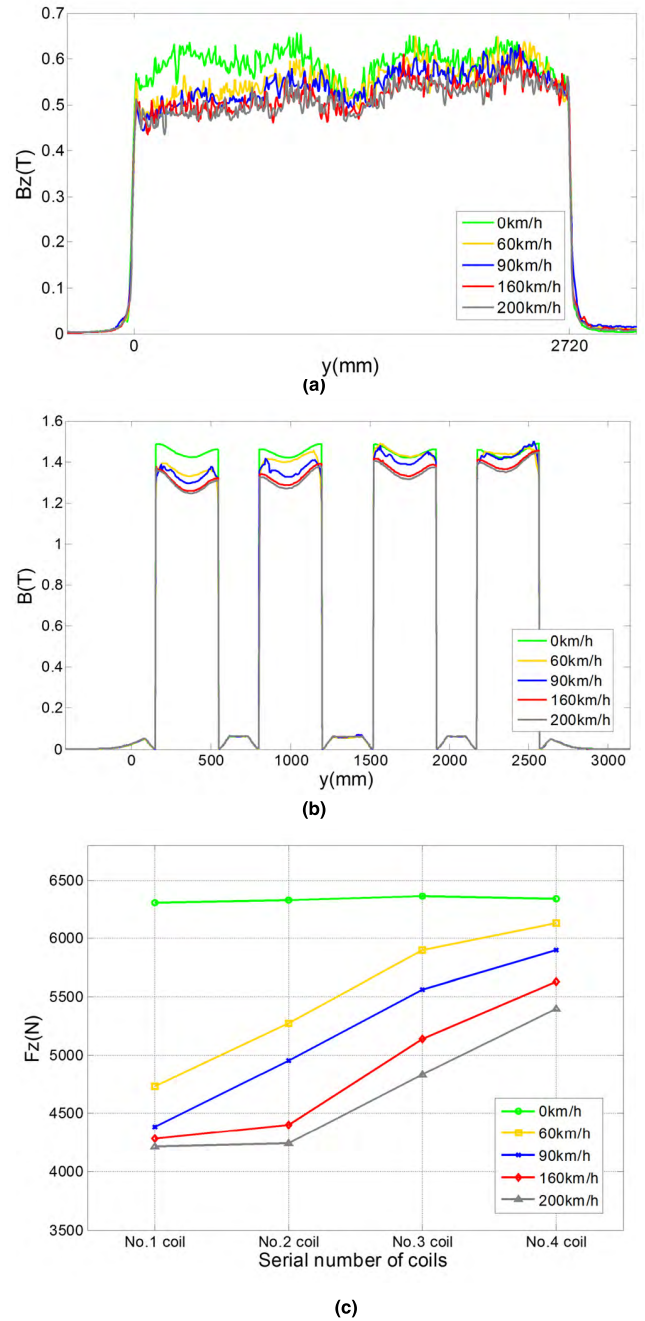

FIGURE 8. (a) Magnetic flux density of air gap in z-direction, (b) magnetic flux density within iron cores at different speeds, (c) Levitation forces Fz provided by each coil.

Fig.8(c) shows the levitation forces provided by each coil at different speeds. The order from the front to the end is coil No.1, No.2, No.3 and No.4 as labeled in Fig.4(a). It can be seen that for the front two coils, the force drops a lot with the decrease of air gap magnetic flux density. For coil No.1, the levitation force decreased by 30% at 90 km/h. Above 90 km/h, the decrease rate of levitation force is much reduced and saturated, and the levitation forces provided by coils

No.1 and No.2 becomes very close. However, the force of coil No.1 still drops by approximately 40 % at 200 km/h.

TABLE 1. F_Z and $\Delta F_Z/F_{Z(0\,km/h)}$ at different speeds of four-coil electromagnet module without levitation control compensation.

Speed	F rail		U rail	
	F_z	$\Delta F_z/F_{z(0km/h)}$	F_z	$\Delta F_z/F_{z(0km/h)}$
0km/h	24954 N	—	24989 N	—
60km/h	21841 N	-12.47%	22538 N	-9.81%
90km/h	20895 N	-16.27%	21807 N	-12.73%
160km/h	19406 N	-22.23%	20345 N	-18.58%
200km/h	18790 N	-24.70%	19816 N	-20.70%

Table 1 shows the levitation forces (F_z) and the drop rates of levitation compared to 0km/h ($\Delta F_z/F_{z(0km/h)}$) of single electromagnet module at different speeds from both F-rail and U-rail models. It can be seen clearly that the F_z results of U-rail are smaller than those from F-rail, and there are around 4% differences between the two sets of $\Delta F_z/F_{z(0km/h)}$ results, which means that it is inappropriate to replace the F-rail with the U-rail as a simplified calculation model. From F-rail model results, at 200 km/h, the eddy current effect reduces the module levitation force by 24.7%. In addition, as the speed increases, the reduction rate of $\Delta F_z/F_{z(0km/h)}$ becomes smaller.

The above analysis is based on the condition that the current of all four coils is 28 A, so that the effect of the eddy current can be seen clearly. However, the actual operation with control is to keep the air gap and levitation force constant, and the influence of eddy effect is compensated by regulating the levitation currents through the controllers. We have some measured current data from CME. Those current data are average values when the train runs at a constant speed. At the steady operation, the force balance will be met. By keeping the air gap magnetic field from falling, we can obtain the required compensation current for force balance in the 3-D FEM simulation. The input current values in the simulation are listed in Table 2. It can be seen that the FEM models produce very close currents compared with those measured in CME. The measured current is slightly larger as there are also vertical forces generated by the head vehicle air dynamics and also the SLIM [22]. Both effects cannot be reflected in the 3-D FEM in our study. This set of data verifies the feasibility of 3-D numerical analysis, and the required compensation current at medium-speed is predicted. When the speed is 200 km/h, the current of coil No.1 and No.2 is 39.8 A.

1) MULTIPLE-MODULE RESULTS

It is also very important to find out the eddy current effect between adjacent electromagnet modules. The FEM model is shown in Fig. 9(a). Fig. 9(b) indicates the air gap magnetic flux density of the model at different speeds. y = 0 is the front of the first module, y = 2888 is the front of the second

TABLE 2. Compensated levitation current at different speeds of four-coil electromagnet module with levitation control compensation.

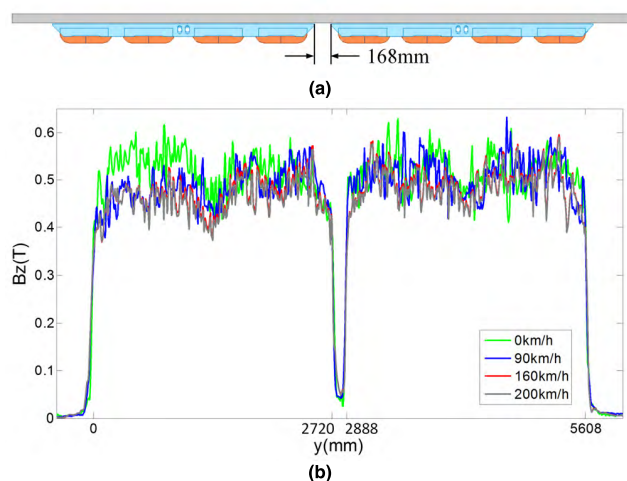| Speed	Simulation		Measurement	
	No.1 and 2	No.3 and 4	No.1 and 2	No.3 and 4
0km/h	28 A	28 A	28 A	28 A
60km/h	32.2 A	28 A	34 A	28 A
90km/h	35 A	28 A	37 A	28 A
160km/h	37.6 A	28 A	—	—
200km/h	39.8 A	28 A	—	—

FIGURE 9. (a) Two-module numerical analysis model; (b) Air gap magnetic flux density of two-module model at different speeds.

module. It can be seen that the second electromagnet module is very limitedly affected by the eddy current effect, because the first electromagnet module has magnetized the rails. When the second electromagnet module arrives, the magnetic field varies much smaller. So the eddy current will become much less significant. The air gap magnetic field at the front of the second module will be very limitedly weakened as shown.

V. AN OPTIMIZED EMS SYSTEM DESIGN

It can be seen from the simulation results that, when the maglev train is running at a speed of 200 km/h, the current in the coils No.1 and No.2 goes far beyond the rating in order to compensate the eddy effect. So an idea of lengthening electromagnet module is proposed to provide larger levitation force and decrease the force burden on each coil. A five-coil electromagnet module scheme is presented. Its structure and control method are shown in Fig.10. The same two-controller system is used as the previous four-coil electromagnet module. When the load remains the same, the five-coil electromagnet module has an extra coil to share the levitation force, so each coil's current will be considerably reduced. Although the weight of the electromagnet is increased, it is negligible compared with the weight of the overall carriage. Since the
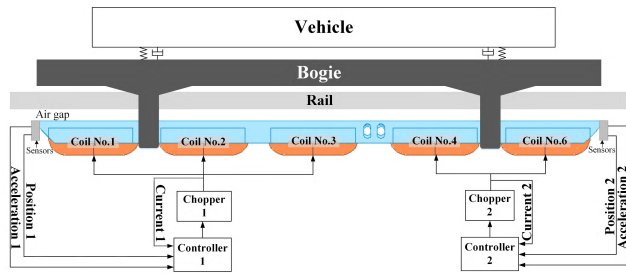
FIGURE 10. Two-controller levitation system of five-electromagnet module.

previous analysis has indicated that the electromagnet modules at the ends of each carriage have serious eddy current effect, only the leading ends of the train need to be installed five-electromagnet modules.

We still take AW0 working condition as the analysis object for comparison with previous four-coil system. The AW0 static levitation current of five-electromagnet module is 24.5 A. Table 3 illustrates the levitation force F_z of single five-electromagnet module at different speeds without levitation control. As the five-coil electromagnet module increases the weight of the electromagnet, some allowance is left for the levitation force, so the value for levitation force when the train stops is 25.56 kN. The drop rate $\Delta F_z/F_{z(0km/h)}$ of the five-coil electromagnet module is consistent with that of the four-coil electromagnet module. However, the drop of force due to eddy current effect corresponding to each coil is reduced.

TABLE 3. F_z and $\Delta F_z/F_z$ (0 km/h) at different speeds of five-coil electromagnet module without levitation control compensation.

Speed	F rail	
	F_z	$\Delta F_z/F_{z(0km/h)}$
0km/h	25561 N	—
60km/h	22292 N	-12.79%
90km/h	21358 N	-16.44%
160km/h	20005 N	-21.74%
200km/h	19117 N	-25.21%

The compensation current required by the five-coil electromagnet module with levitation control under AW0 is also predicted using the previous method as listed in Table IV. When the speed reaches 200 km/h, the current of the first three coils is 34 A, which does not exceed its rated current. It can be seen that the five-coil electromagnet module significantly mitigates eddy current effect while still maintaining the required levitation force.

VI. DISCUSSION

This paper comprehensively analyzes the eddy current effect of the EMS medium-speed maglev train and puts forward a solution. However, there are still some issues that need further discussion.

TABLE 4. Compensated levitation current at different speeds of five-coil electromagnet module with levitation control compensation.

Speed	Simulation	
	No.1 ,2 and 3	No.4 and 5
0km/h	24.5 A	24.5 A
60km/h	27.5 A	24.5 A
90km/h	29.7 A	24.5 A
160km/h	31.8 A	24.5 A
200km/h	34.0 A	24.5 A

1) The saturation of electromagnet module needs more investigation, which is helpful to optimize the structure of electromagnet module for higher speed.

2) Although the eddy current effect between adjacent electromagnet modules is demonstrated, they are on the same carriage. Due to different distances, the adjacent electromagnet modules on different carriages (rear end modules in Fig.1(b)) may not reach the same conclusion. Further analysis might need to be done for the eddy current effect for adjacent electromagnet modules between two different carriages.

3) So far, there is no experimental speed test that has been done in such a high speed by using the separated levitation and propulsion maglev type (Japanese HSST, Korean UTM, and Chinese CME). Previous studies focus more on the propulsion side [22], [23] to achieve a larger or longer acceleration. The eddy current effect in the EMS system would also influence the propulsion system, which needs further analysis.

4) As the electromagnet module is lengthened, if the train structure is not changed, the position of the air spring used to transmit gravity may not coincide with the force center of the levitation control point formed by the first three coils. This will cause problems for levitation control and guidance, which needs to be further discussed.

VII. CONCLUSION

In this paper, through a particularly detailed FEM simulation model, the eddy current effect in EMS system is fully analyzed, and the optimization design applicable to 200 km/h maglev train is proposed. Firstly, the mechanism of eddy current effect in EMS system is explained. Secondly, the process of 3-D FEM is introduced. The FEM simulation shows that the calculation of F-rail is more accurate than U-rail, so a simulation model considering the actual structure of F-rail and electromagnet module is established. Then, the single electromagnet module is analyzed utilizing FEM, which verifies the mechanism of eddy current effect. Moreover, the results are almost consistent with the experimental data available. At 200 km/h, the overall levitation force reduction of the electromagnetic module is predicted to be 24%. The levitation force provided by the first levitation point will decrease by as large as 40% which would require around an

over-rated levitation current of 40 A. The influence between adjacent electromagnet modules is also discussed that only the leading end electromagnet modules have serious eddy current effect. Finally, a five-coil electromagnet module is proposed as well as its corresponding control scheme. The proposed design is proven to be very effective in mitigating the eddy current's influence at 200 km/h where the required levitation force at the leading end of maglev train is nicely maintained.

REFERENCES

[1] L. Yan, "Development and application of the Maglev transportation system," *IEEE Trans. Appl. Supercond.*, vol. 18, no. 2, pp. 92–99, Jun. 2008.

[2] X. Sun, B. Su, L. Chen, Z. Yang, X. Xu, and Z. Shi, "Precise control of a four degree-of-freedom permanent magnet biased active magnetic bearing system in a magnetically suspended direct-driven spindle using neural network inverse scheme," *Mech. Syst. Signal Process.*, vol. 88, pp. 36–48, May 2017.

[3] X. Sun, L. Chen, H. Jiang, Z. Yang, J. Chen, and W. Zhang, "High-performance control for a bearingless permanent-magnet synchronous motor using neural network inverse scheme plus internal model controllers," *IEEE Trans. Ind. Electron.*, vol. 63, no. 6, pp. 3479–3488, Jun. 2016.

[4] X. Sun, L. Chen, and Z. Yang, "Overview of bearingless permanent-magnet synchronous motors," *IEEE Trans. Ind. Electron.*, vol. 60, no. 12, pp. 5528–5538, Dec. 2013.

[5] X. Sun, L. Chen, Z. Yang, and H. Zhu, "Speed-sensorless vector control of a bearingless induction motor with artificial neural network inverse speed observer," *IEEE/ASME Trans. Mechatronics*, vol. 18, no. 4, pp. 1357–1366, Aug. 2013.

[6] L. Yan, "The linear motor powered transportation development and application in China," *Proc. IEEE*, vol. 97, no. 11, pp. 1872–1880, Nov. 2009.

[7] H.-W. Lee, K.-C. Kim, and J. Lee, "Review of Maglev train technologies," *IEEE Trans. Magn.*, vol. 42, no. 7, pp. 1917–1925, Jul. 2006.

[8] J. Xu, J. Li, G. Li, and Z. Guo, "Design and preliminary prototype test of a high temperature superconducting suspension electromagnet," *IEEE Trans. Appl. Supercond.*, vol. 25, no. 2, pp. 1–6, Apr. 2015.

[9] J. Xu, Q. Geng, Y. Li, and J. Li, "Design, fabrication, and test of an HTS magnetic suspension experimental system," *IEEE Trans. Appl. Supercond.*, vol. 26, no. 6, Sep. 2016, Art. no. 3601506.

[10] Q. Yang and J. Li, "Influence of eddy current induced in steel rails on suspension force of EMS high-speed maglev system," in *Proc. 36th Chin. Control Conf. (CCC)*, Dalian, China, Jul. 2017, pp. 10333–10337.

[11] J. Jeong, C.-W. Ha, J. Lim, and J. Choi, "Analysis and control of electromagnetic coupling effect of levitation and guidance systems for semi-high-speed maglev train considering current direction," *IEEE Trans. Magn.*, vol. 53, no. 6, Jun. 2017, Art. no. 8300204.

[12] J.-H. Jeong, C.-W. Ha, J. Lim, and J.-Y. Choi, "Analysis and control of the electromagnetic coupling effect of the levitation and guidance systems for a semi-high-speed MAGLEV using a magnetic equivalent circuit," *IEEE Trans. Magn.*, vol. 52, no. 7, Jul. 2016, Art. no. 8300104.

[13] S.-K. Liu, B. An, S.-K. Liu, and Z.-J. Guo, "Characteristic research of electromagnetic force for mixing suspension electromagnet used in low-speed maglev train," *IET Electr. Power Appl.*, vol. 9, no. 3, pp. 223–228, Mar. 2015.

[14] X. Sun, Y. Shen, S. Wang, G. Lei, Z. Yang, and S. Han, "Core losses analysis of a novel 16/10 segmented rotor switched reluctance BSG motor for HEVs using nonlinear lumped parameter equivalent circuit model," *IEEE/ASME Trans. Mechatronics*, vol. 23, no. 2, pp. 747–757, Apr. 2018.

[15] J. Du and H. Ohsaki, "Numerical analysis of eddy current in the EMS-Maglev system," in *Proc. 6th Int. Conf. Elect. Mach. Syst. (ICEMS)*, Beijing, China, vol. 2, Nov. 2003, pp. 761–764.

[16] S. Yamamura and T. Ito, "Analysis of speed characteristics of attracting magnet for magnetic levitation of vehicles," *IEEE Trans. Magn.*, vol. 11, no. 5, pp. 1504–1507, Sep. 1975.

[17] Y. Li and W. Chang, "Cascade control of an EMS maglev vehicle's levitation control system," *Acta Autom. Sinca*, vol. 119, no. 6A, pp. 946–949, Feb. 1999.

[18] A. Suebsomran, "Optimal control of electromagnetic suspension EMS system," *Open Autom. Control Syst. J.*, vol. 6, no. 1, pp. 1–8, Mar. 2014.

[19] X. Sun, Z. Shi, L. Chen, and Z. Yang, "Internal model control for a bearingless permanent magnet synchronous motor based on inverse system method," *IEEE Trans. Energy Convers.*, vol. 31, no. 4, pp. 1539–1548, Dec. 2016.

[20] W. Barie and J. Chiasson, "Linear and nonlinear state-space controllers for magnetic levitation," *Int. J. Syst. Sci.*, vol. 27, no. 11, pp. 1153–1163, Apr. 1996.

[21] Z. Liu, Z. Long, and X. Li, *Maglev Trains*. Berlin, Germany: Springer, 2015. [Online]. Available: https://www.springer.com/cn/book/9783662456729

[22] Q. Lu, Y. Li, Y. Ye, and Z. Q. Zhu, "Investigation of forces in linear induction motor under different slip frequency for low-speed maglev application," *IEEE Trans. Energy Convers.*, vol. 28, no. 1, pp. 145–153, Mar. 2013.

[23] J. Lim, J.-H. Jeong, C.-H. Kim, C.-W. Ha, and D.-Y. Park, "Analysis and experimental evaluation of normal force of linear induction motor for maglev vehicle," *IEEE Trans. Magn.*, vol. 53, no. 11, pp. 1–4, Nov. 2017.

JINGFANG DING received the B.S. degree in automation from Northeastern University, Shenyang, China, in 2016. She is currently pursuing the master's degree with the National University of Defense Technology, Changsha, China. Her research interests include magnetic levitation control, electromagnetic analysis, control theory, and control engineering.

XIN YANG received the B.Eng. degree from the Huazhong University of Science and Technology, Wuhan, China, in 2009, the M.Sc. degree (Hons.) from Imperial College London, London, U.K., in 2010, and the Ph.D. degree from the University of Cambridge, Cambridge, U.K., in 2014.

He is currently an Assistant Professor with the National University of Defense Technology, Changsha, China. His research interests mainly include high-power semiconductor device modeling and simulation and control of high-power semiconductor devices in power electronic circuits.

Dr. Yang was a recipient of the Cambridge Overseas Scholarship, the Henry Lester Scholarship, the IEEE IES Studentship, and the Cambridge University Lundgren Fund. He was elected as a Huxiang Youth Talent of Hunan Province in 2016.

ZHIQIANG LONG received the B.S. degree in automation from the Huazhong University of Science and Technology, Wuhan, China, in 1988, the M.S. degree in flight mechanics from the Harbin Institute of Technology, Harbin, China, in 1991, and the Ph.D. degree in control science and engineering from the National University of Defense Technology, Changsha, China, in 2010.

He was with the National University of Defense Technology as a Professor, where he is currently the Head Research Engineer of the Engineering Research Center of Maglev Technology. His research interests include magnetic levitation control, fault diagnosis, tolerant control for maglev trains, and new maglev technology.

NING DANG received the B.S. degree from Shanghai Tongji University in 2010. He is currently with the Hunan Maglev Technology Research Center, Changsha, China. His main research directions include maglev-train electrical design, levitation control design, electromagnet design, and magnetic field simulation analysis.

• • •